JOURNAL OF MATERIALS SCIENCE **38** (2003) 2337–2346

Microstructural evolution of brazing 422 stainless steel using the BNi-3 braze alloy

C. L. OU, R. K. SHIUE*
Department of Materials Science and Engineering, National Dong Hwa University, Hualien 974, Taiwan, Republic of China
E-mail: rkshiue@mail.ndhu.edu.tw

The 422 stainless steel (422SS) is one of the typical martensitic stainless steels with both excellent creep strength and corrosion resistance up to 650°C. Its application includes steam turbine blades, high temperatures bolting . . . etc. Repair welding of 422SS is one of the most common methods to fix the turbine blade. However, repair brazing of surface shallow cracks, e.g., less than 1 mm in depth, is an alternative way to fix such blades. The microstructural evolution of brazing 422SS with BNi-3 braze alloy using both infrared and furnace brazing was performed in the study. Based on the experimental results, BNi-3 cannot effectively wet 422SS substrate below 1025°C. As the brazing temperature increases above 1050°C, comprehensive wetting can be obtained in 1200 sec. For the infrared brazed specimen with a short brazing time, the cooling path starts from the formation of a BNi_3 phase in the molten braze, subsequently forms a Ni-rich phase, and finally a eutectic phase is solidified from the residual eutectic liquid. The microstructure of the furnace-brazed specimen is similar to that of infrared brazed specimen, but the interfacial reaction zone is significantly increased in furnace brazing. There are Kirkendall voids in the braze close to the interface between BNi-3 and 422SS, and the size of Kirkendall porosity is increased with increment of the brazing time and/or temperature. The homogenization treatment of the brazed joint at 900°C results in growth of both the interfacial reaction zone and porosity.

1. Introduction

The importance of martensitic stainless steels is increasing in recent years due to the demand from power generation industry [1–3]. It's successful application in corrosive and/or high temperature environment, e.g., high temperature steam pipes, steam turbine blades, rotors . . . etc., has been widely reported in the literatures [1, 4–6]. The 422 stainless steel (422SS) is one of the representative martensitic stainless steel. It is designed for service temperatures up to 650°C, and resistance to oxidation and scaling is good in continuous service at temperature up to 760°C [7]. Excellent mechanical properties can be developed with proper heat treatment of the 422SS [7]. Therefore, it is an excellent alloy characterized with both good creep strength and corrosion resistance. Applications of the 422SS include buckets and blades in compressors and steam turbines, high temperature bolting, compressor and turbine wheel, valves and valve trim, and aircraft parts [7]. Therefore, many researchers have focused on the mechanical properties, fatigue resistance, and corrosion resistance of the 422SS [8–14].

Both the high-pressure and intermediate-pressure steam turbine blades in fossil power plant are primarily made of the 422SS. The carbon content of this alloy is high, and it is alloyed with many other elements, such as Cr, Mo, V, W . . . etc., resulting in high hardenability of the steel. Therefore, the 422SS is difficult to weld due to crack sensitivity [7]. Some studies have been established in welding and/or repair welding of the 422SS [9, 10, 15–18]. Repair welding of 422SS is one of the most common methods to fix such turbine blades. However, the repair welding of shallow cracks on the tips of turbine blades is not the only choice. Repair brazing of surface shallow cracks, e.g., less than 1 mm in depth, is an alternative way to fix the blades. Therefore, both processes are complementary to each other.

Brazing produces coalescence of materials by heating them to the brazing temperature in the presence of a filler metal having a liquidus above 450°C and below the solidus of base metal [19–21]. This study proposes repair brazing of 422 stainless steels, and two primary repair brazing technology will be developed including traditional furnace brazing and infrared brazing. Infrared brazing utilizes infrared energy generated by heating a tungsten filament in a quartz tube as the heating source, and it is featured with a very fast heating rate up to 3000°C/min [22–24]. The infrared rays can

*Author to whom all correspondence should be addressed.

TABLE I Summary of the process variables used in the experiment

Furnace type	Temperature (°C)	Time (sec)	Environment	Heating rate (°C/min)
Infrared furnace	1050	60, 180, 300	Vacuum	600°C/min
Traditional furnace	1050[a]	600, 1200, 1800	Vacuum	30°C/min
Traditional furnace	1075[a]	600, 1200, 1800	Vacuum	30°C/min
Traditional furnace	1100[a]	600, 1200, 1800	Vacuum	30°C/min

[a]The specimen was subsequently homogenized at 900°C for 24 and 120 hrs.

transmit through the quartz tube, and not be absorbed by the furnace itself. Consequently, local heating of the bonding surfaces can be acquired by using an appropriate optical focusing system. Infrared brazing is a very promising technology among all brazing processes [22–24].

Nickel base braze alloys are featured with good corrosion resistance and creep strength, so they are good choices in repair brazing of 422SS. BNi-3 is a nickel base braze alloy, and its chemical composition in weight percent is 3.1 B, 4.5 Si, 0.06 C (max) and Ni balance. The solidus temperature of BNi-3 is 980°C, and its liquidus temperature is 1040°C [19]. The brazing temperature of BNi-3 braze is between 1010°C and 1175°C, and the suggested brazing temperature of BNi-3 alloy is 1040°C [19]. The range of 422SS austenitizing temperature is between 1040°C and 1055°C, so it is preferred that the repair brazing temperature of 422SS is below 1055°C [7]. Accordingly, the suggested brazing temperature of BNi-3 is very close to the austenitizing temperature of 422SS. Therefore, BN-3 was chosen as the brazing filler metal in the study.

The purpose of this investigation is concentrated on the repair brazing of 422SS using both infrared brazing and furnace brazing. A nickel base braze alloy, BNi-3, was used as brazing filler metal. The effect of process variables, e.g., brazing temperature, brazing time and homogenization time . . . etc., on the microstructural evolution of the brazed joint will be extensively evaluated.

2. Experimental procedure

The base metal used in the experiment was 422SS disk with the diameter of 32 mm and thickness of 3 mm. Its chemical composition in weight percent was 0.24 C, 0.71 Mn, 0.38 Si, 0.016 P, 0.006 S, 0.76 Ni, 11.98 Cr, 1.07 Mo, 0.26 V, 0.99 W and balance Fe. The 422SS specimen was polished by using a SiC paper, and an ultrasonic bath made use of acetone as the solvent to clean the specimen prior to brazing. A nickel base filler metal, Nicrobraz® 130 made by Wall Colmonoy Co., was chosen as the braze alloy in the experiment. According to the specification of American Welding Society (AWS) for Ni base braze alloys, the chemical composition of Nicrobraz® 130 alloy is consistent with BNi-3 braze [19]. The braze alloy was in the form of Nicrobraz® 130 tape with the thickness of 125 μm and 50 mm wide.

Infrared brazing was performed in a vacuum of 5×10^{-5} mbr at 1050°C for 60–300 sec. The heating rate of the infrared furnace was set at 600°C/min throughout the experiment, and the specimen was preheated at 600°C for 600 sec prior to the brazing temperature. Traditional furnace brazing was performed in a vacuum of 5×10^{-5} mbar at temperatures between 1050°C and 1100°C for various time periods. The heating rate of furnace brazing was set at 30°C/min throughout the experiment. All specimens were preheated at 600°C for 600 sec prior to the brazing temperature. In order to study the microstructural evolution of the brazed joint, the furnace brazed specimen was subsequently homogenized at 900°C for 24 and 120 hrs, respectively. The process variables applied in brazing 422SS using BNi-3 (Nicrobraz® 130) filler metal are summarized in Table I.

Dynamic wetting angle measurements were made using the above traditional furnace at the temperature ranges between 1025°C and 1100°C for 0–1800 sec [25, 26]. 0.15 g master alloy was placed on the 422SS substrate, and the heating rate of the furnace was 30°C/min. The image of wetting angle was recorded simultaneously by a camera.

The brazed specimen was cut by a low speed diamond saw, and the specimen subsequently experienced a standard metallographic procedure prior to further inspection. The etching solution used in the experiment was the solution of 50% acetic acid and 50% nitric acid. The cross section of the brazed specimens was firstly examined by using a Hitachi 3500 H scanning electron microscope (SEM) with an accelerating voltage of 15 KV. Quantitative chemical analysis was performed using a JEOL JXL-8800 M electron probe microanalyzer (EPMA) with an operation voltage of 15 KV and spot size of 1 μm.

3. Results and discussions

Fig. 1 shows the dynamic wetting angle measurement of BNi-3 braze on 422SS for 1025–1100°C between 0–1800 sec. Based on the figure, BNi-3 cannot effectively wet 422SS substrate below 1025°C. As the brazing

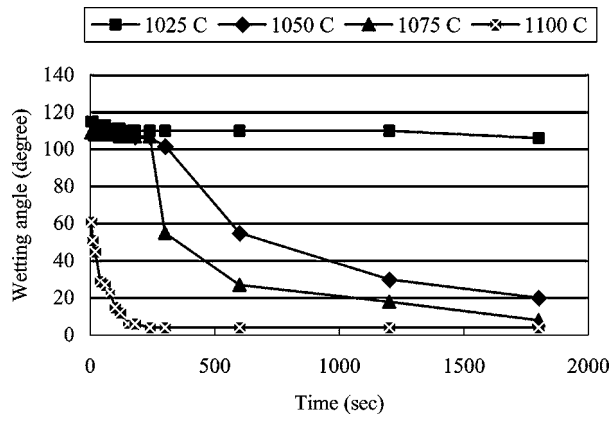

Figure 1 The dynamic wetting angle measurements of BNi-3 braze alloy on 422SS substrate for 1025–1100°C between 0–1800 sec.

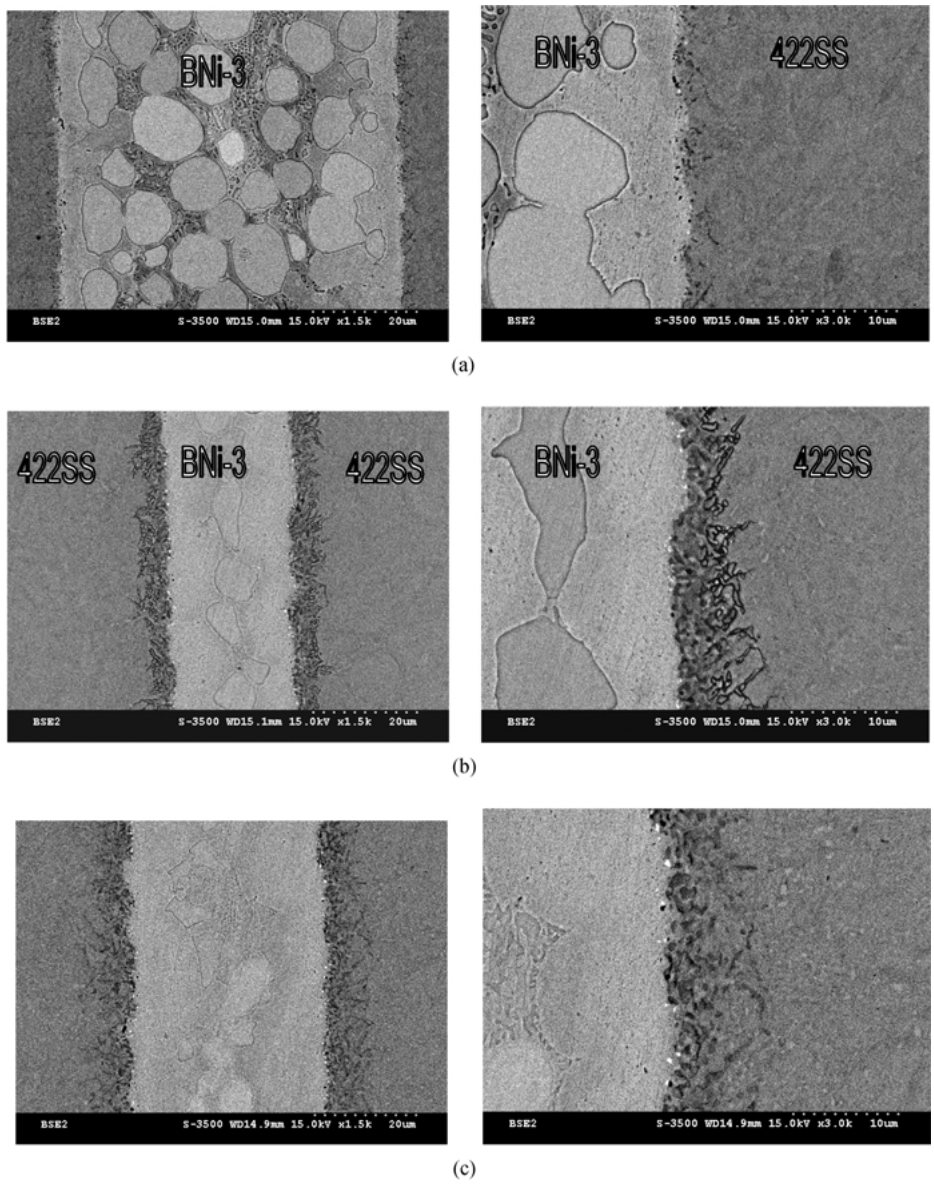

Figure 2 The SEM backscattered images of 422SS infrared brazed at 1050°C for (a) 60, (b) 180, and (c) 300 sec.

temperature increases above 1050°C, the wetting angle is decreased below 30° in 1200 sec. For the specimen brazed at 1100°C, BNi-3 molten braze can spread completely on the 422SS substrate in 200 sec. Since the wettability of BNi-3 braze is insufficient at 1025°C, the brazing of 422SS was performed above 1050°C in the experiment.

Fig. 2 illustrates the SEM backscattered images of 422SS infrared brazed at 1050°C for 60, 180 and 300 sec. The backscattered image does not provide topographic contrast but primarily shows the element distribution in the joint [27]. Consequently, the area of the specimen containing high-atomic number elements appears light, while the area with low-atomic number elements appears dark [27]. It is apparent that the distribution of elements in the brazed joint is not uniform, and there are many phases in the brazed joint. Additionally, there is a reaction layer at the interface between BNi-3 and 422SS as shown in Fig. 2b and c. For the specimen infrared brazed at 1050°C for 60 sec, very limited reaction zone is observed due to insufficient reaction time during infrared brazing as shown in Fig. 2a. On the other hand, thickness of reaction zone between BNi-3 braze and 422SS is increased with increasing the brazing time.

Fig. 3 shows the SEM images and EPMA chemical analyses of the specimen infrared brazed at 1050°C for 60 sec. Point 8 in the figure demonstrates the substrate of 422SS. Point 7 is located at the interface between BNi-3 braze and 422SS, and its chemical composition is mainly comprised of Fe, Cr and Ni. As described earlier, the reaction zone between BNi-3 braze and 422SS is not prominent for short brazing time, so there is no continuous reaction layer at the interface. At least three phases with different chemical compositions are observed in the joint as illustrated by points 1–6 in Fig. 3. A ternary phase diagram, if available, is very helpful in explaining the microstructural evolution of the brazed joint. The chemical composition of BNi-3 braze alloy is primarily composed of Ni, B and Si, so a B-Ni-Si ternary alloy phase diagram is quoted in the study [28].

Fig. 4 displays the partial liquidus projection of the B-Ni-Si ternary alloy phase diagram in atomic percent, and some important invariant reactions are also included in the figure [28]. The cooling path in the ternary alloy phase diagram is valid only if the solidification

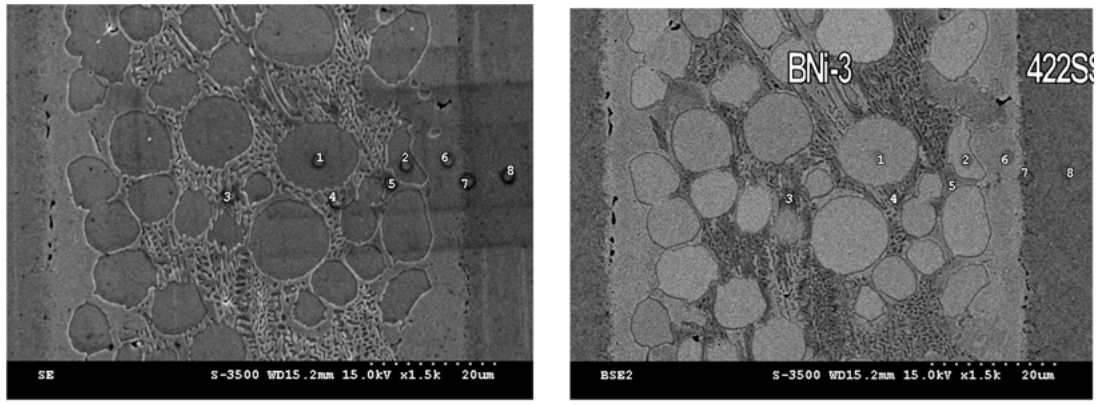

(a) (b)

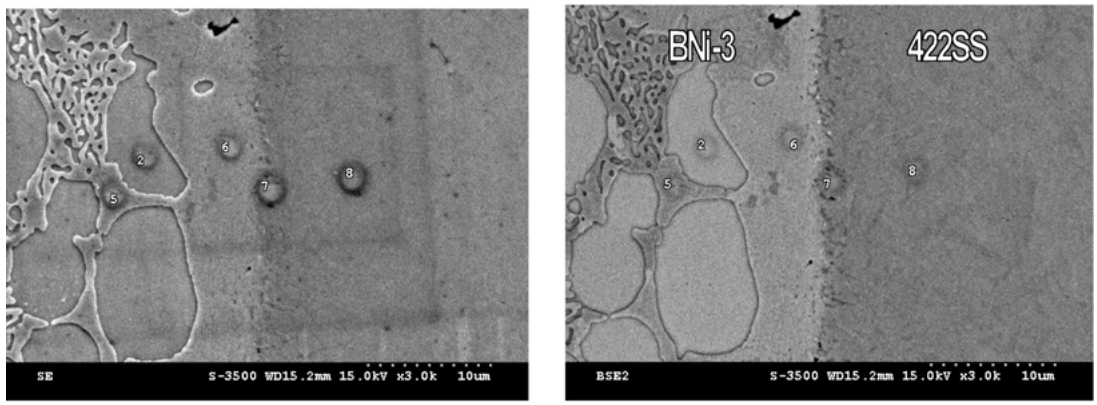

(c) (d)

At%	1	2	3	4	5	6	7	8
B	15.6	15.9	3.1	0.4	0.3	0.0	0.0	0.3
C	2.1	1.9	1.7	2.0	2.6	2.1	2.0	3.1
Si	0.0	0.0	18.0	17.5	12.9	9.8	0.9	0.6
Cr	0.0	0.1	0.1	0.1	0.2	0.9	8.5	13.5
Fe	0.4	1.0	0.6	0.7	1.5	6.9	78.8	79.5
Ni	81.8	81.0	76.5	79.2	82.4	80.0	8.3	1.0
V	0.0	0.0	0.0	0.0	0.0	0.0	0.1	0.2
Mn	0.0	0.0	0.0	0.0	0.0	0.1	0.7	0.7
Mo	0.0	0.0	0.0	0.0	0.0	0.0	0.4	0.7
W	0.0	0.0	0.0	0.0	0.0	0.1	0.2	0.3

Figure 3 The SEM images (a) (c) secondary electron images, (b) (d) backscattered electron images, and EPMA chemical analyses of the specimen infrared brazed at 1050°C for 60 sec.

of the molten brazes is in equilibrium and no reaction between BNi-3 and 422SS. Since infrared brazing is characterized with rapid thermal cycles, very limited interfacial reaction is observed in short brazing cycle. For example, infrared brazing at 1050°C for 60 sec is short enough to depress the interaction between braze and substrate. Therefore, the cooling path predicted by B-Ni-Si ternary alloy phase diagram can be an approximation of the solidified BNi-3 braze. According to Fig. 4, there are two ternary eutectic reactions in the partial B-Ni-Si ternary alloy phase diagram. The chemical composition of BNi-3 in atomic percent is 14.2% B, 7.9% Si and 77.9% Ni, and it is located in the primary field of BNi_3 as marked by A in the figure. Additionally, the point A in Fig. 4 is close to E_1 ternary eutectic reaction, which can be expressed by $L \leftrightarrow BNi_3 + (Ni) + Ni_3Si$ at 993°C [28]. According to the liquidus projection of B-Ni-Si ternary phase diagram, the cooling path of point A in Fig. 4 starts from the formation of a BNi_3 phase in the liquid, subsequently forms a Ni-rich phase in the molten liquid, and finally a eutectic phase is solidified from the residual eutectic liquid.

The chemical compositions of point 1 and 2 in Fig. 3 are rich in boron content, and their composition is close to BNi_3. There is a Ni-rich phase alloyed with Si, Fe, C and Cr as marked by point 6 in the figure. According to Ni-Si and B-Ni binary alloy phase diagram, the maximum solubility of Si in Ni at room temperature is 10 at%, but there is no solubility of B in Ni metal [29]. The composition of point 6 contains 9.8 at% Si, but there is no boron found at point 6. It is considered a Ni-rich phase in the braze. Finally, there is a eutectic phase in the braze as marked by 3 and 4 in Fig. 3. Based on the B-Ni-Si ternary alloy phase diagram, the eutectic phase

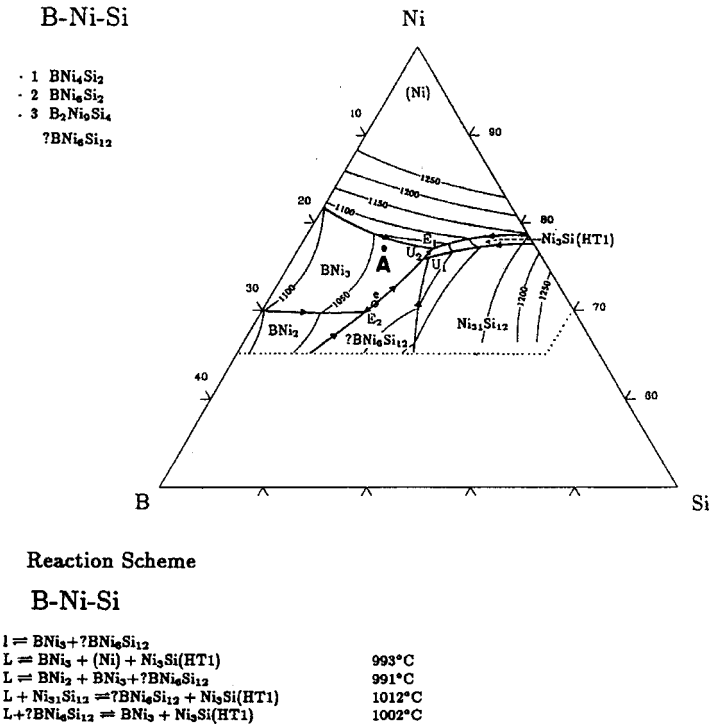

Reaction Scheme

B-Ni-Si

e :	$l \rightleftharpoons BNi_3 + ?BNi_6Si_{12}$	
E_1 :	$L \rightleftharpoons BNi_3 + (Ni) + Ni_3Si(HT1)$	993°C
E_2 :	$L \rightleftharpoons BNi_2 + BNi_3 + ?BNi_6Si_{12}$	991°C
U_1 :	$L + Ni_{31}Si_{12} \rightleftharpoons ?BNi_6Si_{12} + Ni_3Si(HT1)$	1012°C
U_2 :	$L + ?BNi_6Si_{12} \rightleftharpoons BNi_3 + Ni_3Si(HT1)$	1002°C

Figure 4 The partial liquidus projection of B-Ni-Si ternary alloy phase diagram [28].

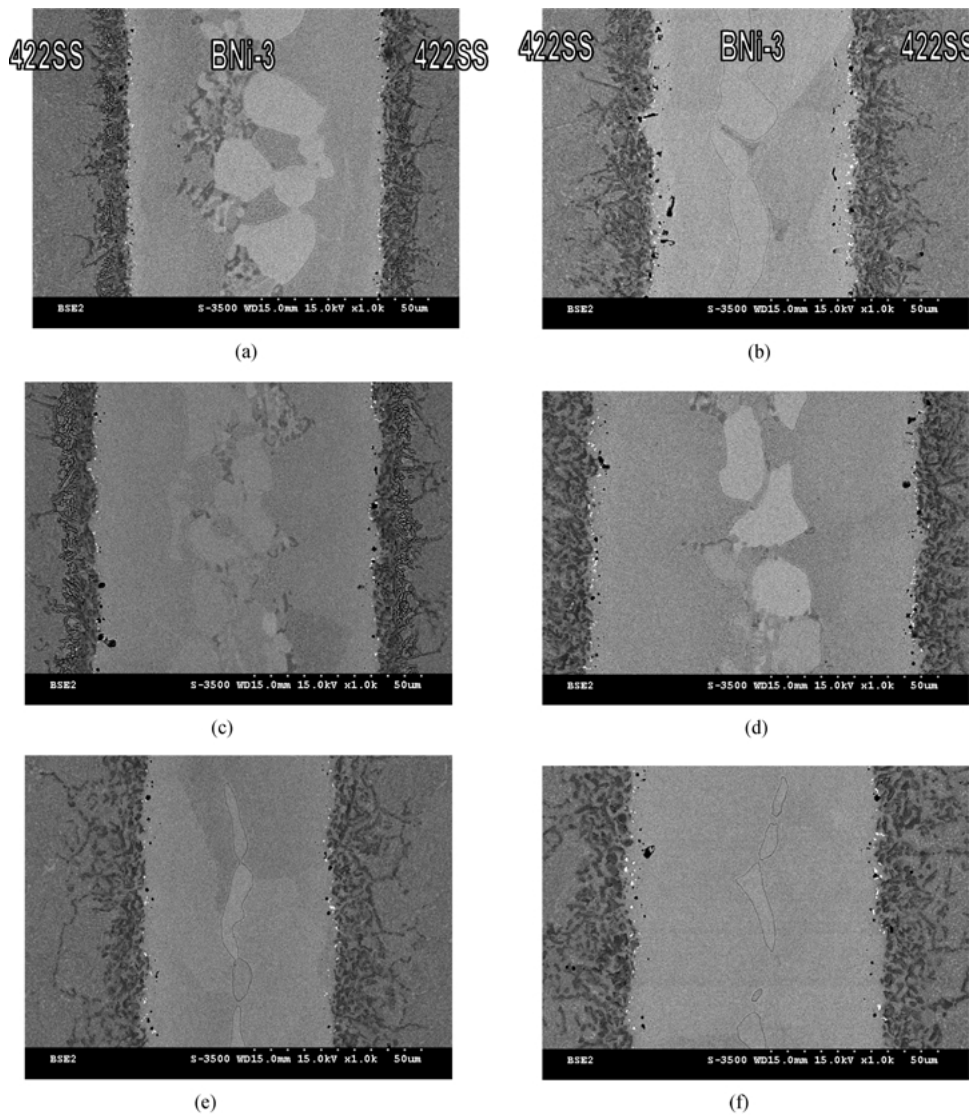

Figure 5 The SEM backscattered images of furnace brazed specimens at (a) 1050°C × 600 sec, (b) 1050°C × 1800 sec, (c) 1075°C × 600 sec, (d) 1075°C × 1800 sec, (e) 1100°C × 600 sec, and (f) 1100°C × 1800 sec.

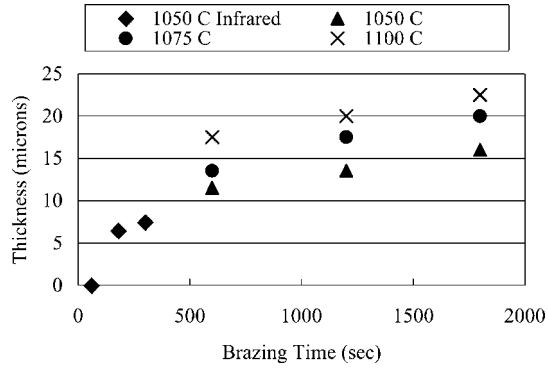

Figure 6 The relation among thickness of the reaction zone, brazing time and brazing temperature.

consists of BNi_3, Ni and Ni_3Si phases, and the chemical composition of point 3 and 4 mainly consists of Ni, Si and B. Consequently, the experimental observation is consistent with the B-Ni-Si ternary phase diagram.

Fig. 5 shows the SEM backscattered images of 422SS furnace brazed at various temperatures. The microstructure of the furnace-brazed specimen is similar to that of infrared brazed specimen with longer brazing time, e.g., 180 and 300 sec. Compared with the infrared brazed specimen, the interfacial reaction zone is greatly increased in the furnace brazing. Fig. 6 summarizes the relation among the thickness of the reaction zone, brazing time and brazing temperature. In the figure, 1050°C Infrared stands for infrared brazing, and all

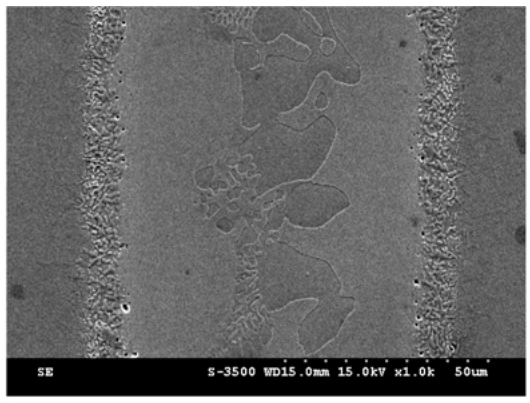

(a)

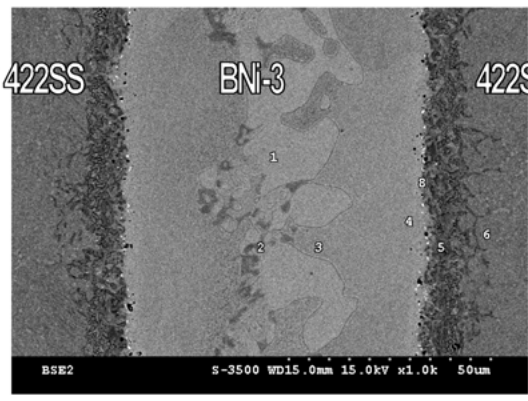

(b)

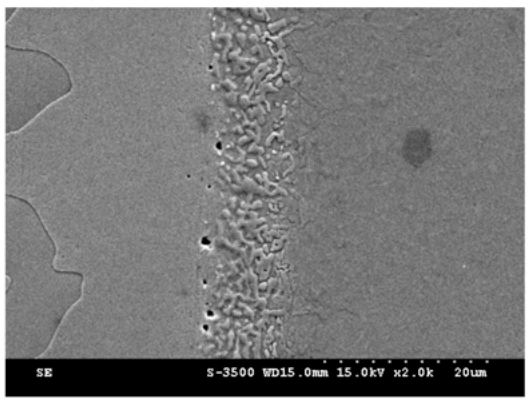

(c)

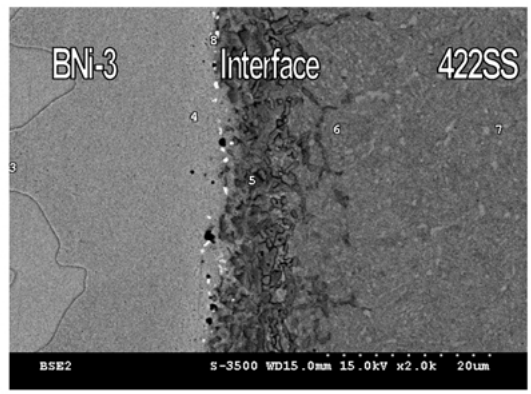

(d)

At	1	2	3	4	5	6	7	8
B	21.4	1.1	1.2	0.0	9.0	1.6	0.0	2.7
C	1.8	1.0	1.8	1.5	2.9	4.1	2.8	4.1
Si	0.1	17.5	11.2	7.8	0.5	0.7	0.7	2.3
Cr	0.6	0.4	1.3	1.9	12.5	12.9	12.4	4.8
Fe	3.8	3.2	8.5	17.2	67.3	78.6	82.1	43.7
Ni	72.4	76.8	75.7	71.4	6.8	0.7	0.7	41.4
V	0.0	0.0	0.0	0.0	0.0	0.1	0.0	0.0
Mn	0.0	0.1	0.2	0.1	0.4	0.6	0.7	0.2
Mo	0.0	0.0	0.0	0.1	0.3	0.5	0.4	0.5
W	0.0	0.0	0.0	0.0	0.2	0.3	0.2	0.2

Figure 7 The SEM images (a) (c) secondary electron image, (b) (d) backscattered electron image, and EPMA chemical analyses of the specimen furnace brazed at 1050°C for 600 sec.

others are traditional furnace brazing at 1050°C, 1075°C and 1100°C, respectively. It is noted that the thickness of the reaction zone is increased with increasing brazing temperature and/or time.

The EPMA chemical analyses were performed for the specimen furnace brazed at 1050°C for 600 sec as displayed in Fig. 7. Different from the specimen infrared brazed at 1050°C for 60 sec, both Fe and Cr contents in the braze are increased due to the enhanced dissolution of 422SS substrate into the molten braze during furnace brazing. The chemical composition of point 1 is close to BNi_3 alloyed with minor other elements. Similar to the aforementioned result, point 2 is the eutectic phase primarily consisting of Ni, Si, B and Fe. Point 4 is the Ni-rich phase alloyed with Fe, Si, Cr and C. Point 5 stands for the composition of the reaction zone between BNi-3 and 422SS, and the interfacial phase is primarily comprised of Fe, Cr, Ni, B and C. It was reported that boron in the nickel-base braze alloy can diffuse promptly into the base metal and form compounds along grain boundaries [24, 30]. Since the chemical composition of point 5 is rich in Fe, Cr, Ni, B and C, it is reasonable that a significant number of borides and/or carbides might be expected in this region.

The boron can diffuse into 422SS substrate via both grain boundary and bulk diffusion as shown in Figs 5 and 7d, and forms the Fe-Cr-B-Ni interfacial phase. Furthermore, there are a few porosities in the braze close to the interface as displayed in Fig. 7c. The porosity is called Kirkendall porosity, and it results from nonsymmetrical mass transport during interdiffusion [31]. The Kirkendall effect describes that the vacancy will be formed if the rate of interdiffusion is not balanced [31]. Since boron is a very small atom, it can diffuse much faster than Fe and Cr atoms with a larger atomic radius. Consequently, boron can readily diffuse into 422SS substrate, but much slower diffusion rates of Fe and Cr atoms from 422SS into the braze are predictable. Some Kirkendall voids (below 2 microns) in the braze close to the interface between BNi-3 and 422SS are found in the figure. The Kirkendall effect is a diffusion-controlled phenomenon, so it is strongly temperature and time dependent. It is expected that the size of Kirkendall porosity is ever increasing with increment of the brazing time and/or temperature due to the enhancement of nonsymmetrical mass transport during interdiffusion.

The reaction between BNi-3 braze alloy and 422SS substrate may cause isothermal solidification of the molten braze during brazing. Because the melting point depressant, e.g., boron in BNi-3 braze alloy, readily diffuses into 422SS, the 422SS is also dissolved into the molten braze during brazing. Both metallurgical phenomena result in increasing the melting point of the molten braze.

The furnace-brazed specimens were subsequently homogenized at 900°C for 24 and 120 hrs in order to confirm the phase stability of the furnace-brazed joint. Fig. 8 shows the SEM backscattered images of the furnace brazed specimens at 1050–1100°C and subsequent homogenization at 900°C for 24 and 120 hrs,

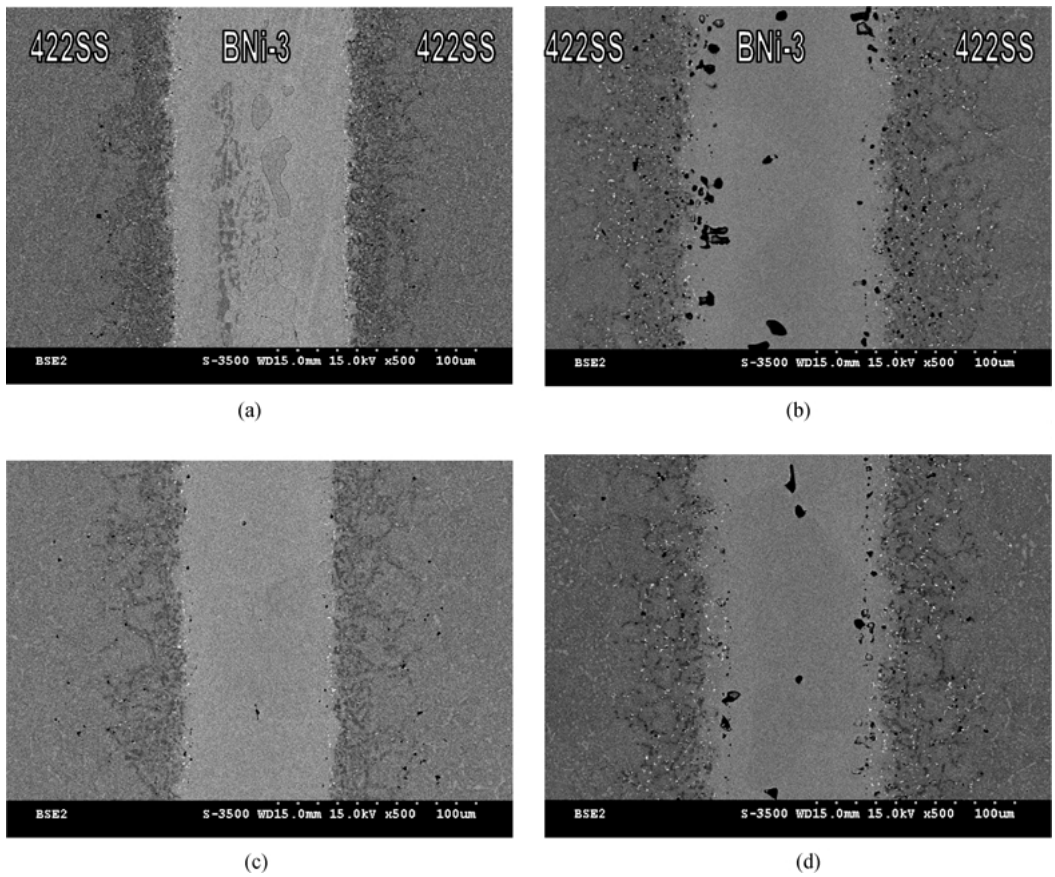

Figure 8 The SEM backscattered images of furnace brazed specimens at 1050°C × 600 sec and 900°C for (a) 24 hrs, (b) 120 hrs, 1100°C × 1800 sec and 900°C for (c) 24 hrs, and (d) 120 hrs.

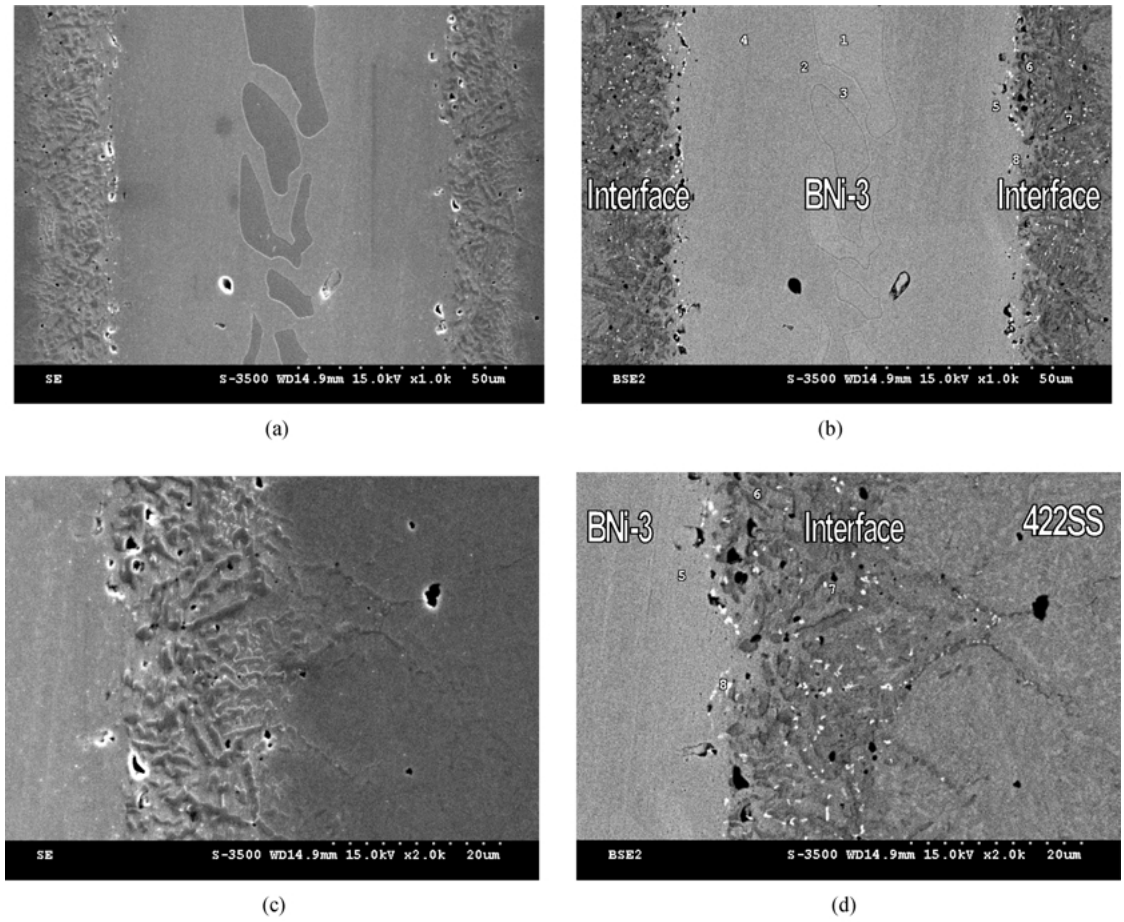

At	1	2	3	4	5	6	7	8
B	20.0	0.0	0.0	1.2	0.0	27.0	22.1	20.9
C	1.3	7.9	1.4	1.4	1.1	0.9	0.8	1.0
Si	0.0	6.5	6.4	6.5	2.9	0.3	0.2	0.7
Cr	0.7	1.1	1.1	1.5	3.3	18.9	12.1	11.3
Fe	4.1	8.1	7.9	14.2	36.4	41.2	60.6	30.1
Ni	73.8	76.2	83.1	74.9	56.0	11.0	2.2	28.5
V	0.0	0.0	0.0	0.0	0.0	0.1	0.1	0.3
Mn	0.0	0.2	0.1	0.2	0.3	0.3	0.6	0.2
Mo	0.0	0.1	0.1	0.0	0.1	0.2	0.8	4.8
W	0.0	0.0	0.0	0.0	0.0	0.2	0.4	2.3

Figure 9 The SEM images (a) (c) secondary electron images, (b) (d) backscattered electron images, and EPMA chemical analyses of the specimen furnace brazed at 1050°C for 600 sec and homogenization at 900°C for 24 hrs.

respectively. It is possible that Kirkendall porosity is located close to the center of the braze due to the disappearance of BNi_3 phase in the braze alloy after homogenization for long time periods, e.g., 24 and 120 hrs as shown in Fig. 8b and d. The depletion of boron content from the braze alloy results in the formation of Kirkendall porosity. It is apparent that the longer homogenization time will cause enhanced Kirkendall effect. Consequently, many voids are observed in the braze as displayed in Fig. 8b and d.

Fig. 9 illustrates both the SEM images and EPMA chemical analyses of the specimen furnace brazed at 1050°C for 600 sec and followed by homogenization at 900°C for 24 hrs. The BNi_3 phase is still observed as marked by 1 in Fig. 9, but the eutectic phase is now disappeared. The growth of reaction zone results in depletion of boron content from the braze. It is expected that the boron containing phase in braze is decreased with increasing homogenization time of the brazed joint. The braze alloy is mainly composed of the Ni-rich phase alloyed with many other elements as marked by points 2–4 in Fig. 9. Additionally, high Fe content of the Ni-rich phase close to the interface is observed at point 5 of Fig. 9. Similarly, the interfacial reaction zone mainly consists of Fe, Cr, B and Ni as demonstrated by point 6 and 7 in Fig. 9.

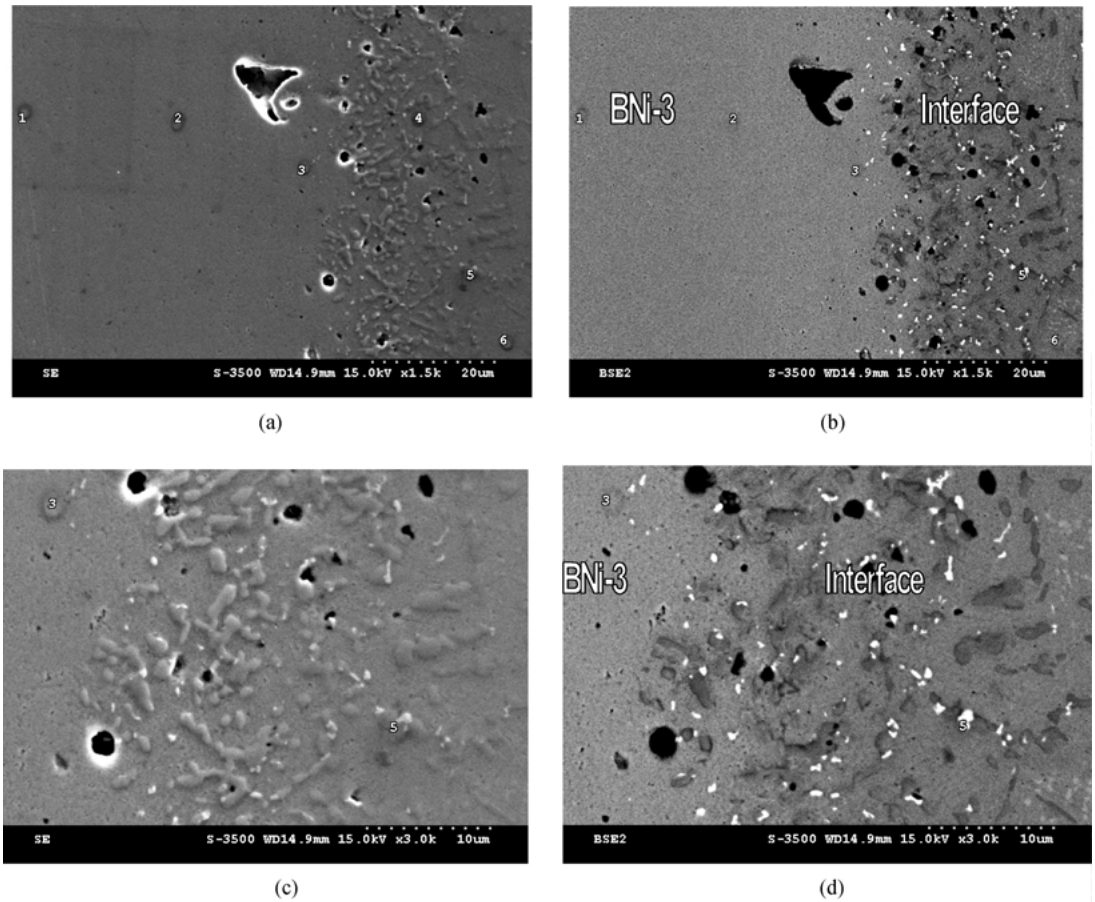

At%	1	2	3	4	5	6
B	0.0	0.0	0.0	1.0	11.1	1.9
C	1.8	1.9	1.4	2.4	1.0	3.6
Si	8.6	6.5	3.0	0.8	0.5	0.7
Cr	2.0	3.0	5.9	7.5	15.9	10.9
Fe	17.6	23.7	43.2	84.3	69.4	80.2
Ni	69.6	64.6	45.7	3.2	0.6	0.6
V	0.0	0.1	0.1	0.0	0.2	0.1
Mn	0.4	0.2	0.4	0.6	0.8	0.7
Mo	0.1	0.1	0.2	0.2	0.4	0.7
W	0.0	0.0	0.3	0.0	0.1	0.6

Figure 10 The SEM images (a) (c) secondary electron images, (b) (d) backscattered electron images, and EPMA chemical analyses of the specimen furnace brazed at 1050°C for 600 sec and homogenization at 900°C for 120 hrs.

According to the EPMA analyses of the light particle shown in Fig. 9 (point 8), its chemical composition in atomic percent is roughly 20.9% B, 1.0% C, 0.7% Si, 11.3% Cr, 30.1% Fe, 28.5% Ni, 0.3% V, 0.2% Mn, 4.8% Mo and 2.3% W. Therefore, these very light particles can be classified as a type of boride primarily containing B, Cr, Fe, Ni, Mo and W. Additionally, 4.8 at% Mo are equal to 9.0 wt% Mo, and 2.3 at% W are equal to 8.2 wt% W. The amount of Mo and W in the light particle is as high as 10 wt%, respectively. High atomic number of both W and Mo results in high brightness of the BSE image in SEM observations. Since the chemical composition of 422SS contains Mo and W, these light particles are located at the interface between the braze and 422SS substrate due to dissolution of 422SS substrate during brazing.

Fig. 10 shows the SEM images and EPMA chemical analyses of the specimen furnace brazed at 1050°C for 600 sec and followed by homogenization at 900°C for 120 hrs. The BNi_3 phase is completely vanished in the braze due to the depletion of boron, and the chemical composition of the braze matrix is free of boron as marked by 1–3 in the figure. According to the EPMA chemical analysis of point 5 in Fig. 10, there are Fe-Cr-B borides in the reaction zone. The growth of these boride precipitates during homogenization of the brazed joint results in depletion of the boron content in the braze alloy. The boron containing phase in the braze is not stable upon homogenizing the brazed joint at 900°C, so the BNi_3 phase in the matrix is disappeared after homogenization of the joint at 900°C for 120 hrs. Therefore, Kirkendall porosity is

observed nearby the interface. In comparison among Figs 7c, 9c and 10c, the size of Kirkendall porosity is increased with increasing homogenization time. The homogenization treatment of the brazed joint results in growth of both the interfacial reaction zone and porosity.

4. Conclusions

The microstructural evolution of brazing 422SS using BNi-3 (Nicrobraz® 130) braze alloy was performed in the study. In addition to traditional furnace brazing, infrared repair brazing of 422SS was also included in the study. The experimental result can be summarized as below.

1. BNi-3 cannot effectively wet 422SS substrate below 1025°C. As the brazing temperature increases above 1050°C, the wetting angle is below 30° in 1200 sec. For the specimen brazed at 1100°C, BNi-3 molten braze can spread completely on 422SS substrate in 200 sec.

2. The braze alloy is primarily comprised of BNi_3, a Ni-rich phase and a eutectic phase after infrared brazing. There is a reaction zone primarily comprised of Fe, Cr, B and Ni. For the specimen infrared brazed at 1050°C for 60 sec, very limited reaction zone is observed due to insufficient reaction time during brazing. On the other hand, the thickness of the reaction zone between BNi-3 braze and 422SS is rapidly increased with increasing the brazing temperature and/or time.

3. The microstructure of the furnace brazed specimen is similar to that of infrared brazed specimen with longer brazing time, but the thickness of interfacial reaction zone is significantly increased for the furnace brazed specimen due to longer brazing time.

4. There is Kirkendall porosity in the braze close to the interface between BNi-3 and 422SS substrate, and the size of Kirkendall porosity is ever increasing with increment of the brazing time and/or temperature.

5. Both Kirkendall porosity and interfacial reaction zone cannot be removed by homogenization of the brazed joint at 900°C. On the contrary, the homogenization treatment of the brazed joint at 900°C results in growth of both the interfacial reaction zone and Kirkendall voids.

Acknowledgements

The authors gratefully acknowledge the financial support of this research by the National Science Council (NSC), Republic of China under grant numbers: NSC 90-2216-E-259-003 and NSC 91-2216-E-259-002. EPMA analysis by Ms. Shu-Yueh Tsai in NSC Instrument Center, National Tsing Hua University, Hsin-Chu, Taiwan, is also gratefully acknowledged.

References

1. A. HIZUME, Y. TAKEDA, H. YOKOTA, Y. TAKANO, A. SUZUKI, S. KINOSHIA, M. KOONO and T. TSUCHIYAMA, *J. Eng. Mater. Tech.* **109** (1987) 319.
2. M. C. BALMFORTH and J. C. LIPPOLD, *Welding J.* **77** (1998) 1s.
3. R. B. CORBIT and S. M. FRENCH, *ibid.* **76** (1997) 51.
4. D. ARMSTRONG, *Welding in the World* **31** (1993) 426.
5. C. E. CHANG, *Trans. Geothermal Resources* **13** (1989) 569.
6. M. E. ABD, M. M. GHONEIM, A. M. NASRELDIN and S. SOLIMAN, *J. Eng. Appl. Sci.* **44** (1997) 183.
7. H. CHANDLER, "Heat Treater's Guide: Practice and Procedures for Irons and Steels" (ASM International, Materials Park, Ohio, 1995) p. 777.
8. M. K. LEE, *J. Nuclear Mate.* **254** (1998) 42.
9. P. K. LIAW, J. ANELLO, N. S. CHERUVU and J. K. DONALD, *Metall. Trans.* **15A** (1984) 693.
10. P. R. LANDON, R. D. CALIGIURI and P. S. DULETSKY, *ibid.* **14A** (1983) 1395.
11. C. R. BROOKS and F. BOGNI, *Mater. Charact.* **38** (1997) 103.
12. J. R. SCULLY and H. S. SCULLY, *Corrosion* **49** (1993) 99.
13. C. R. BROOKS and J. P. ZHOU, *Metallography* **23** (1989) 27.
14. F. V. ELLIS and S. TORDONATO, *Trans. ASME J. of Pressure Vessel Tech.* **22** (2000) 66.
15. P. WOOLLIN, *Welding Research Abroad* **41–44** (1995) 34.
16. W. WU, L. Y. HWU, D. Y. LIN and J. L. LEE, *Scripta Mater.* **42** (2000) 1071.
17. H. Y. HAN and Z. SUN, *International J. Pressure Vessels and Piping* **60** (1994) 59.
18. B. J. GINN and T. G. GOOCH, *Welding J.* **77** (1998) 341s.
19. D. L. OLSON, T. A. SIEWERT, S. LIU and G. R. EDWARDS, "ASM Handbook, Welding, Brazing, and Soldering," Vol. 6 (ASM International, Metals Park, Ohio, 1993).
20. M. SCHWARTZ, "Brazing: For the Engineering Technologist" (Chapman & Hall, New York, 1995) p. 1.
21. G. HUMPSTON and D. M. JACOBSON, "Principles of Soldering and Brazing" (ASM International, Metals Park, Ohio, 1993) p. 1.
22. T. Y. YANG, S. K. WU and R. K. SHIUE, *Intermetallics* **9** (2001) 341.
23. R. K. SHIUE, S. K. WU, J. M. O. and J. Y. WANG, *Metall. Mater. Trans.* **31A** (2000) 2527.
24. R. K. SHIUE, S. K. WU and C. M. HUNG, *ibid.* **33A** (2002) 1765.
25. C. C. LIN, R. B. CHEN and R. K. SHIUE, *J. Mater. Sci.* **36** (2001) 2145.
26. R. B. CHEN and R. K. SHIUE, *J. Mater. Sci. Lett.* **20** (2001) 1435.
27. R. E. LEE, "Scanning Electron Microscopy and X-Ray Microanalysis" (Prentice Hall, New York, 1993) p. 130.
28. P. VILLARS, A. PRINCE and H. OKAMOTO, "Handbook of Ternary Alloy Phase Diagrams" (ASM International, Metals Park, Ohio, 1995) p. 5508.
29. T. B. MASSALSKI, "Binary Alloy Phase Diagrams" (ASM International, Materials Park, Ohio, 1990).
30. A. RABINKIN, E. WENSKI and A. RIBAUDO, *Weld. J.* **77** (1998) 66s.
31. G. HUMPSTON and D. M. JACOBSON, "Principles of Soldering and Brazing" (ASM International, Metals Park, Ohio, 1993) p. 127.

Received 30 July 2002
and accepted 27 February 2003